Macromolecules

Article

pubs.acs.org/Macromolecules

Supramolecular Magnetic Brushes: The Impact of Dipolar Interactions on the Equilibrium Structure

Pedro A. Sánchez,*[,†] Elena S. Pyanzina,[‡] Ekaterina V. Novak,[‡] Joan J. Cerdà,[§] Tomas Sintes,[§] and Sofia S. Kantorovich[†,‡]

[†]University of Vienna, Sensengasse 8, 1090, Vienna, Austria

[‡]Ural Federal University, Lenin av. 51, 620000, Ekaterinburg, Russia

[§]Instituto de Física Interdisciplinar y Sistemas Complejos, IFISC (CSIC-UIB), E-07122 Palma de Mallorca, Spain

ABSTRACT: The equilibrium structure of supramolecular magnetic filament brushes is analyzed at two different scales. First, we study the density and height distributions for brushes with various grafting densities and chain lengths. We use Langevin dynamics simulations with a bead−spring model that takes into account the cross-links between the surface of the ferromagnetic particles, whose magnetization is characterized by a point dipole. Magnetic filament brushes are shown to be more compact near the substrate than nonmagnetic ones, with a bimodal height distribution for large grafting densities. This latter feature makes them also different from brushes with electric dipoles. Next, in order to explain the observed behavior at the filament scale, we introduce a graph theory analysis to elucidate for the first time the structure of the brush at the scale of individual beads. It turns out that, in contrast to nonmagnetic brushes, in which the internal structure is determined by random density fluctuations, magnetic forces introduce a certain order in the system. Because of their highly directional nature, magnetic dipolar interactions prevent some of the random connections to be formed. On the other hand, they favor a higher connectivity of the chains' free and grafted ends. We show that this complex dipolar brush microstructure has a strong impact on the magnetic response of the brush, as any weak applied field has to compete with the dipole−dipole interactions within the crowded environment.

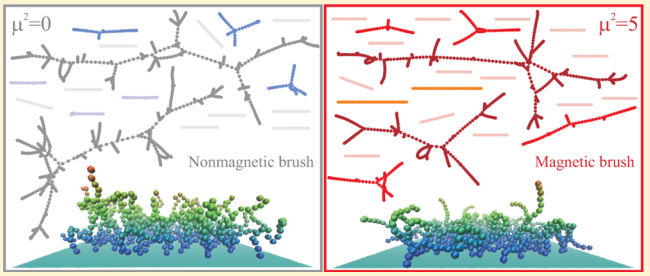

INTRODUCTION

Polymer brushes consist of a relatively dense layer of macromolecular chains tethered to a surface by one of their ends.[1,2] These systems can be designed to obtain a convenient modification of the properties of the underlying surface, leading to their control at the submicrometric scale. In general, the properties of the brushes strongly depend on the interplay between the intrinsic properties of the individual polymer chains and the constraints introduced by the presence of the substrate and the neighboring chains. This gives polymer brushes a rich structural landscape and, consequently, a broad range of potential applications, currently being used as a key approach for the creation of advanced soft matter systems and nanotechnologies.[3] For instance, among the most well-established applications of polymer brushes, we can find the control of the flocculation of colloidal particles,[4] the design of filtration and separation systems,[5] and the control of the adsorption and sensing of biomolecules.[6,7]

Besides the simple tuning of the properties of material surfaces, in recent years there has been a growing interest in the use of polymer brushes for the creation of responsive interfaces, i.e., surfaces whose properties may change or adapt to the environmental conditions and/or exhibit a controlled response to external stimuli. For example, it is possible to achieve the spontaneous modification of the brushes' structures and their swelling properties according to the nature of the solvent,[8,9] the switchable functionalization of their free surfaces controlled by the background temperature[10] or pH,[11] and their use as mechanical nanosensors and actuators.[12] Among the diverse stimuli that may control the structure of responsive surfaces, the use of external fields is particularly appealing for technological applications. As a well-known example, electric fields can be used to modify the structure of brushes made out of polyelectrolytes.[13−16] Another attractive approach is the creation of brushes with a response to external magnetic fields. The control of the interface properties by means of external magnetic fields provides an evident advantage, especially for applications in which the system interacts with substances that are undesirably sensitive to electric fields and/or to other potential control parameters, such as the background temperature or pH. However, in difference with polyelectrolytes, polymers with a significant magnetic response are far less common substances. To date, only polymers that exhibit magnetic properties at very low temperature have been possible to synthesize.[17,18] Nevertheless, the creation of a magnetoresponsive surface can be achieved by applying more sophisticated approaches.

Received: May 20, 2015
Revised: September 8, 2015
Published: October 12, 2015

DOI: 10.1021/acs.macromol.5b01086
Macromolecules 2015, 48, 7658−7669

Some of the most advanced techniques for the design of responsive surfaces include the incorporation of colloidal particles into the system in order to facilitate the control of their functional and/or structural properties. In particular, the incorporation of magnetic colloids into polymer brush-like structures is a promising strategy to obtain a magnetoresponsive behavior. Despite their potential interest, to our best knowledge just a few studies on the design of such magnetoresponsive supramolecular nanostructures exist to date.[19,20] In such works, the magnetic colloids are simply embedded into a polymer brush without a fine control of their locations and moment orientations. Here, we propose an alternative design of a magnetoresponsive brush-like system, based on the replacement of the tethered polymer chains by supramolecular magnetic filaments, i.e., by polymer-like chains of prealigned ferromagnetic colloids that have been permanently cross-linked by means of macromolecules in order to keep their chain structure under a broad range of conditions.[21−25] Magnetic filaments grafted to one end to a surface have been used in recent years to work as micro- and nanofluidic pumps and mixers,[26−31] either alone or in sparse arrays. In this work we explore the possibility of increasing the grafting density of such tethered magnetic filaments to form a brush-like structure at a supramolecular scale, with ferromagnetic colloids playing the role of polymer monomers. We expect this system to have a much higher and controllable magnetic response than the aforementioned polymer brushes loaded with magnetic particles in a less organized way. In particular, we focus on the study of the equilibrium structural properties of the filament brush as the first step to determine the potential of this system for practical applications. With this goal, we perform extensive Langevin dynamics simulations with a bead−spring model of the filament brush that takes into account the cross-links between the surface of the colloids. We analyze its equilibrium structures for different grafting densities and filament lengths and determine the effects of the long-range magnetic dipolar interactions by means of a comparison with non magnetic filament brushes. We also compare our results with previous theoretical works on brushes of neutral polymers and polyelectrolytes with extended electric dipoles. Finally, we introduce a graph theory based analysis approach—to our best knowledge, novel in this context—in order to characterize the internal structure of the brush. We found that the magnetic filament brush, for high enough grafting densities, is split into two well-pronounced structural regions: near the substrate, it is very compact, albeit its internal structure is less interlaced and more anisotropic in comparison to a nonmagnetic filament brush; the upper part of the brush is composed by dangling chain free ends. We also observed that our model for the cross-links within supramolecular filaments introduces significant differences in the overall brush structure with respect to what is found in conventional bead−spring models of molecular neutral polymers and polyelectrolytes with extended electric dipoles. These differences make the magnetic filament brush to exhibit a higher magnetization and a more pronounced change in its thickness, when exposed to external fields, than the ones shown by polyelectrolyte brushes with extended electric dipoles or embedded magnetic colloids.

The paper is organized as follows: in the next section, we describe the model of the brush used in our computer simulations; next, we study the overall structural properties of the brush—i.e., its structure at the scale of complete filaments; a higher resolution—corresponding to the scale of individual beads—is then used to explain the unusual behavior brought to the system by the long-range magnetic dipolar interactions; finally, the manuscript ends with a brief summary.

FILAMENT BRUSH MODEL AND SIMULATION METHOD

In recent works we introduced a phenomenological bead−spring model of magnetic filaments that represents a chain of permanently cross-linked monodisperse ferromagnetic colloids, whose magnetic moments have an orientation fixed with respect to the colloid solid body structure.[32,33] The cross-links are assumed to consist of polymers attached to the surface of neighboring particles, created when the colloids are in a straight chain disposition with a head-to-tail arrangement of their magnetic moments. Current experimental techniques allow the tuning of the length of the cross-linkers in a rather broad range.[25,34]

Briefly, our model represents the colloids as soft core spheres with a characteristic diameter d and a point magnetic dipole moment $\vec{\mu}$ located at their center. We take into account the long-range magnetic interactions between the beads by means of the conventional dipole−dipole pair potential:

$$U_{dd}(\vec{r}_{ij};\vec{\mu}_i,\vec{\mu}_j)=\frac{\vec{\mu}_i\cdot\vec{\mu}_j}{r_{ij}^{\,3}}-\frac{3(\vec{\mu}_i\cdot\vec{r}_{ij})(\vec{\mu}_j\cdot\vec{r}_{ij})}{r_{ij}^{\,5}} \tag{1}$$

where $r_{ij}=|\vec{r}_{ij}|$, being $\vec{r}_{ij}=\vec{r}_i-\vec{r}_j$ the displacement vector connecting the centers of beads i and j with dipolar moments $\vec{\mu}_i$ and $\vec{\mu}_j$ respectively. It is worth noting that introducing point dipoles—an exact representation for the case of magnetic single domain colloids—provides a substantial difference from early models of polyelectrolytes, in which extended electric dipoles where introduced by alternating the sign of the monomer electric charges.[35] In particular, the point dipoles located at the particles centers introduce a strong anisotropy in the interactions at the scale of individual particles, without regard to the (in)existence of a permanent connectivity between them.

The soft core steric interaction between the beads is modeled with a Weeks−Chandler−Andersen pair potential (WCA),[36]

$$U_{\mathrm{WCA}}(r)=\begin{cases}U_{\mathrm{LJ}}(r)-U_{\mathrm{LJ}}(r_{cut}), & r<r_{\mathrm{cut}}\\ 0, & r\geq r_{\mathrm{cut}}\end{cases} \tag{2}$$

where $U_{\mathrm{LJ}}(r)$ is the conventional Lennard-Jones potential

$$U_{\mathrm{LJ}}(r)=4\epsilon_s[(d/r)^{12}-(d/r)^{6}] \tag{3}$$

and $r_{\mathrm{cut}}=2^{1/6}d$ is the shifting parameter that makes the potential purely repulsive. The constraining effects of the cross-linkers that bond any pair of neighboring particles are represented by a simple harmonic spring whose ends are attached to the surface of both soft spheres, i.e., to points at a distance $d/2$ from the sphere centers. The locations of such attachment points correspond to the projections of the head and the tail of the magnetic moments of every bead. Figure 1a shows a scheme of this linking potential, whose expression is

$$U_S(\vec{r}_{ij};\hat{\mu}_i,\hat{\mu}_j)=\frac{1}{2}K_S\left(\vec{r}_{ij}-(\hat{\mu}_i+\hat{\mu}_j)\frac{d}{2}\right)^2 \tag{4}$$

where $\hat{\mu}_i=\vec{\mu}_i/\|\vec{\mu}_i\|$ and $\hat{\mu}_j=\vec{\mu}_j/\|\vec{\mu}_j\|$ are the unitary vectors parallel to each associated dipole moment. We want to underline that this linking model is also significantly different from the usual spring models applied to molecular

DOI: 10.1021/acs.macromol.5b01086
Macromolecules 2015, 48, 7658−7669

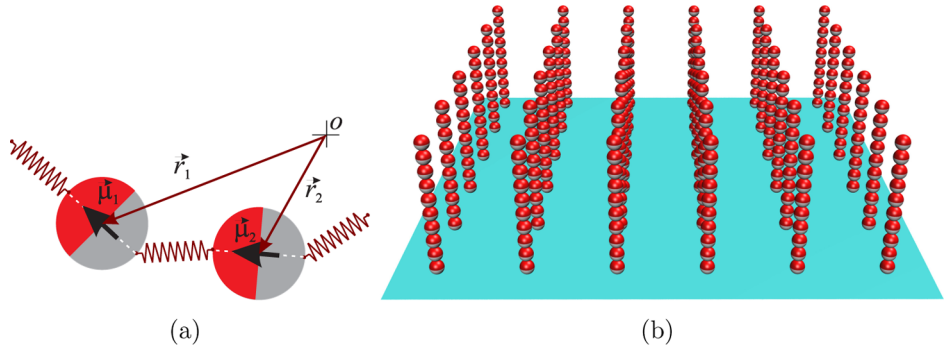

Figure 1. (a) Schematic representation of the links between neighboring magnetic beads used in our filaments model. The orientation of the dipoles is indicated by both the black arrows and the red and gray colors of the beads. (b) Example of an initial filament brush configuration, corresponding to filaments of length $N = 10$ and a grafting density of $\sigma = 0.027$.

polymers—typically, finitely extensible nonlinear elastic springs.[37] Such springs only provide an isotropic constraint to the center to center distance between the beads. Here, instead, we aim at representing accurately the effect of the cross-linkers which, being anchored to the surface of the colloids, also constrain the rotational degrees of freedom. The combination of potentials 2 and 4 favors the arrangement of the dipoles into a head-to-tail alignment parallel to the chain backbone, thus making the filaments locally more straight than isotropic spring-linked chains and, consequently, highly magnetoresponsive.[33] We expect this model to be a more accurate representation of A-type Stockmayer polymers, i.e., polymers with monomer dipoles being aligned along the backbone, than that of extended fluctuating dipoles made out of point charges.[35] The model also differs significantly from other coarse-grained models of cross-linked superparamagnetic colloids,[38,39] i.e., particles in which the dipole moment is not coupled to the chain backbone.

For simplicity, in this work, we measure all the physical parameters of the system in reduced units, taking as reference the reduced characteristic diameter of the colloids, $d = 1$, their reduced mass $m = 1$, and the prefactor of the reduced steric potential 2, $\epsilon_s = 1$. According to our previous works, the prefactor of the potential 4 is set to $K_s = 30$, a value that provides average bond lengths close to the reference bead soft core diameter $(d = 1)$ and a maximum distance between two bonded particle surfaces to be approximately half of the particle diameter. Finally, we take $\mu^2 = (\vec{\mu}\cdot\vec{\mu}) = 5$ for the squared dipole moment of the magnetic filament beads. These values for the interparticle interaction parameters correspond to for example, magnetite spheres with a magnetic core diameter of approximately 25−30 nm coated with a 5−10 nm polymer shell, which is also used to cross-link the particles.

Finally, the filament brush is modeled in the following way. First, a set of identical filaments with N beads each is placed in a cubic simulation box of side length L, with periodic boundary conditions in the x and y directions to mimic an infinite horizontal brush size. Every chain is grafted by fixing the position of one of its end beads close to a flat steric surface located at $z = 0$. The steric repulsion produced by this surface on the beads is given by a truncated shifted 9−3 Lennard-Jones potential,[40] which is obtained by applying expression 2 to

$$U_{\mathrm{LJ}}^{9-3}(r) = \frac{3\sqrt{3}}{2}\left[\left(\frac{d}{2r}\right)^9 - \left(\frac{d}{2r}\right)^3\right] \tag{5}$$

where r is in this case the z coordinate position of the bead center. The potential 5 is the result of integrating a conventional 12−6 Lennard-Jones potential over an infinite flat surface. The position of its minimum determines a new cutoff, $r_{\mathrm{cut}} = 3^{1/6}d/2$, to which the z position of the fixed end particle is permanently set. The orientation of the dipole of this fixed end particle is also set to permanently remain pointing in the z direction. The rest of the filament beads are initially disposed in a perfect head-to-tail arrangement perpendicular to the surface. The horizontal positions of the grafting points are placed in a square lattice of separation constant a. Therefore, the number grafting density of the brush, σ, defined as the number of grafting points per unit of grafting surface area, is given by $\sigma = a^{-2}$. Figure 1b shows, as an example, the initial configuration of a brush of filaments with length $N = 10$ and grafting density $\sigma = 0.028$.

With this filament brush model, extensive computer simulations were performed for different values of N and σ by means of the ESPResSo 3.2.0 simulation package.[41,42] In order to avoid the explicit simulation of the background fluid, we chose the Langevin dynamics (LD) simulation method.[43] In LD simulations, the effect of the background fluid is treated implicitly by introducing stochastic terms in the translational and rotational equations of motion that apply to each particle i

$$m_i\frac{\mathrm{d}\vec{v}_i}{\mathrm{d}t} = \vec{F}_i - \Gamma_T\vec{v}_i + \vec{\xi}_{i,T},$$
$$\mathbf{I}_i\cdot\frac{\mathrm{d}\vec{\omega}_i}{\mathrm{d}t} = \vec{\tau}_i - \Gamma_R\vec{\omega}_i + \vec{\xi}_{i,R}, \tag{6}$$

where $\vec{F}_i$ and $\vec{\tau}_i$ are the total force and torque, m_i is the mass, $\mathbf{I}_i$ the inertia tensor, and Γ_T and Γ_R the translational and rotational friction constants, respectively. Finally, $\vec{\xi}_{i,T}$ and $\vec{\xi}_{i,R}$ are respectively a Gaussian random force and torque that satisfy the usual fluctuation−dissipation relations, namely, they have a zero mean value and a variance equal to $2\Gamma_l T$, where $\Gamma_l = \{\Gamma_T, \Gamma_R\}$ and T is the reduced temperature.[44] The values of the dynamical parameters—i.e., mass, inertia tensor, and friction constants—are physically irrelevant for the determination of the equilibrium properties of the system. Thus, we take $\Gamma_T = 1$ and $\Gamma_R = 3/4$ as values known to produce a conveniently fast relaxation to equilibrium in this type of simulation.[45,46] Finally, in order to ensure isotropic rotations, an identity matrix is taken for the inertia tensor. Another important choice is the method to compute the dipole−dipole interactions, due to their long-range nature. In a relatively dense system of magnetic dipoles with periodic boundaries, the use of

DOI: 10.1021/acs.macromol.5b01086
Macromolecules 2015, 48, 7658−7669

a simple cutoff approach might be unacceptably inaccurate. Therefore, we chose to use the dipolar-P^3 M method,[47] specifically designed to accurately compute the magnetic dipolar interactions of pseudoinfinite systems, in combination with the dipolar layer correction method.[48] The latter is required to take into account the slab geometry of our system, i.e. the absence of periodic boundaries in the z direction.

The simulation protocol we used is the following. First, for each simulation run, the background temperature of the system, measured in reduced units, was set to $T = 1$. Then, an initial configuration for a given set of values of N and σ was created and a first pre-equilibration cycle was performed without computing the dipolar interactions, i.e., by taking $\mu^2 = 0$. This pre-equilibration cycle consisted of a progressive increment of the integration time step, from 10^{-8} to 10^{-5}, in 10 subcycles of 5×10^5 timesteps each. For $\mu^2 = 5$, a second analogous pre-equilibration cycle was then performed to progressively increase the dipolar moment of the beads from 10^{-10} to its final value. Once such pre-equilibration cycles were completed, an equilibration cycle of 10^7 timesteps and a final cycle of measures were performed. The length of the equilibration cycle was chosen to ensure that both the average and the variance of the energy and the mean-square total magnetic moment were able to reach the saturation. In every run, 20 measures were taken at intervals of 10^6 timesteps. Finally, a minimum of five independent runs were performed for every set of explored parameters.

PROPERTIES ON THE FILAMENT SCALE

In order to determine the effect of the dipolar interactions on the equilibrium structure of the filament brush, we first analyze two conventional overall chain parameters: the density profile and the distribution of chain heights.

Brush Density Profiles. The number density distribution of chain monomers as a function of the distance to the grafting surface, $\phi(z)$, is a common parameter used to characterize brush-like structures.[49] In this case, we compute this parameter for the positions of the bead centers. Figure 2 shows the results of $N\,\phi(z)$ obtained for two selected values of chain length and grafting density, for nonmagnetic ($\mu^2 = 0$, squares) and magnetic filaments ($\mu^2 = 5$, filled circles). The main plots correspond to the profiles calculated for the whole set of particles in the system, whereas, in the insets only the particles located at the free ends of the chains have been considered. We multiply them by N to make the scales along ordinate comparable. The data is plotted as a function of the height normalized with the characteristic contour length of the filaments, $z^* = z/(N-1)d$. As predicted by the Semenov–Milner–Witten theory (SMW), and as is found in conventional models of polymer brushes,[37] the nonmagnetic brush has an approximately parabolic profile, corresponding to the following expression[50]

$$\phi(z) \sim -z^2 + \text{const} \tag{7}$$

The main plots show an excellent agreement in the least-squares fit of this function to the simulation data at heights larger than $z^* \gtrsim 0.3$. More importantly, Figure 2 also illustrates the existence of a significant difference in the behavior of magnetic brushes: without exception, the magnetic brush has a more compact structure than the nonmagnetic one, with a higher density close to the grafting surface and a lower density far from it. A shift of the density profile toward the substrate was also found in models of polyelectrolytes with extended

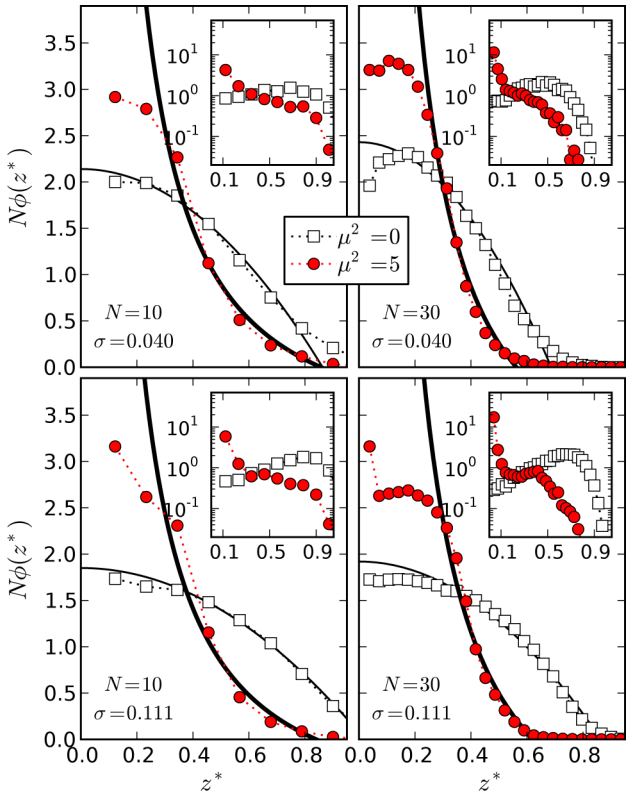

Figure 2. Examples of density profiles corresponding to the combination of two chain lengths (N = 10, 30) and two grafting densities (σ = 0.04, 0.111). Main figures show the profiles of the whole brush structure. Inset figures, plotted in semilogarithmic scale, correspond to the distribution of the free end beads of the filaments. Solid thin and thick lines in the main figures are, respectively, the fits of eqs 7 and 8 to the rightmost range of the simulation data. Squares correspond to $\mu^2 = 0$; filled circles to $\mu^2 = 5$.

dipoles.[35] In our case, we observe the decay of density in the upper region to deviate from a parabolic behavior when dipoles are present. Instead, a least-squares fit of the de Gennes self-similar carpet profile[49,51]

$$\phi(z) \sim z^{-1.3} + \text{const} \tag{8}$$

shows a good agreement with the simulation data for $z^* \gtrsim 0.4$. The profile for the free ends is also significantly different in the dipolar brush. While the nonmagnetic chains keep most of their free ends far from the grafting surface, as predicted by the SMW model,[50] the main part of the magnetic free ends is found to be in close contact with it. This means that the dipolar interactions within the brush prevent the filaments to reach their normal entropic extension in the z direction, leading to a more compact overall brush structure with a clear −1.3-power scaling. At this point one might wonder if the filaments are forming individual closed loops to minimize the magnetic flux, as is known to happen to dipolar chains under conditions of strong intrachain dipolar interactions in front of the thermal fluctuations and other non intrachain interactions.[52−56] However, the calculation of the probability distribution for the normalized end-to-end distance of the chains, $R^*_{ee} = |\vec{r}_1 - \vec{r}_N|/(N-1)d$, shown in Figure 3 for a given chain length and grafting density, proves that there exists just a slight increase of closed chains in the dipolar case with respect to the nonmagnetic one, being in both cases a very small fraction in the system. Therefore, the internal structure of the magnetic brush is more complex than

DOI: 10.1021/acs.macromol.5b01086
Macromolecules 2015, 48, 7658−7669

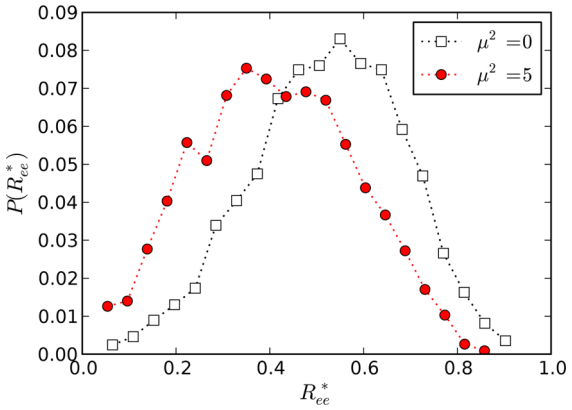

Figure 3. Probability distributions of the normalized end-to-end distance obtained for magnetic (μ^2 = 5, filled circles) and non magnetic (μ^2 = 0, open squares) brushes with chain length N = 30 and grafting density σ = 0.040.

the one given by a simple closure of the chains. This points to the relevance of the dipolar interchain interactions in the structure of the magnetic brushes.

Finally, we make a comparison of our density profiles with earlier models of brushes of neutral polymers and polyelectrolytes with extended dipoles.[35,37] Following the latter, for this purpose we calculate the normalized average brush height, $\langle z^* \rangle$, from the first moment of the density profile:

$$\langle z^* \rangle = \frac{1}{d(N-1)} \frac{\int_0^\infty \phi(z) z \, dz}{\int_0^\infty \phi(z) \, dz} \tag{9}$$

Table 1 shows the values of this parameter for selected values of chain length, grafting density and dipole moment. By

Table 1. Selected Values of the Average Height of Magnetic and Nonmagnetic Filament Brushes, $\langle z^* \rangle_{\mu^2=5}$ and $\langle z^* \rangle_{\mu^2=0}$ Respectively, Obtained for Different Chain Lengths and Grafting Densities

N	σ	$\langle z^* \rangle_{\mu^2=0}$	$\langle z^* \rangle_{\mu^2=5}$	$100\left(1-\frac{\langle z^* \rangle_{\mu^2=5}}{\langle z^* \rangle_{\mu^2=0}}\right)$, %
10	0.040	0.41	0.32	22
10	0.111	0.46	0.31	33
30	0.040	0.28	0.20	29
30	0.111	0.35	0.23	34

calculating the ratio $\langle z^* \rangle_{\mu^2=5}/\langle z^* \rangle_{\mu^2=0}$, we can see that the relative decrease in the brush height introduced by the dipolar interactions increases with both the chain length and the grafting density, ranging roughly from 22 to 34%. This behavior is different from the case of polyelectrolyte brushes with extended dipoles: as shown by the study of Kaznessis and co-workers,[35] the influence of the electric dipoles becomes less pronounced as the grafting density increases, showing a change from 10 to 5% for the same range of parameters. One can assume that the qualitative difference in the physical behavior of a magnetic filament brush compared to a brush consisting of polyelectrolyte chains with alternating charges stems from the fact that in the latter system, with increasing grafting density, the interaction that mainly determines the internal structure of a brush is the central Coulomb interaction between individual point charges, rather than the dipolar one. In contrast, for a magnetic filament brush, the directionality of the dipole−dipole interaction is enhanced when the bead density grows and, consequently, the average distance between the point dipoles is reduced.

Distribution of Mean Chain Heights. Further insight on the overall structure of the brush can be obtained by looking at the probability distribution of filament mean heights, $P(\langle h_c \rangle)$, where $\langle h_c \rangle$ is the average z position of the centers of every bead i belonging to a given filament, $\langle h_c \rangle = (1/N) \sum_{i=1}^{N} z_i$. This parameter will tend to a value of one-half of the characteristic contour length of the chains for a brush formed by vertically straight filaments. Figure 4a shows the probability distributions

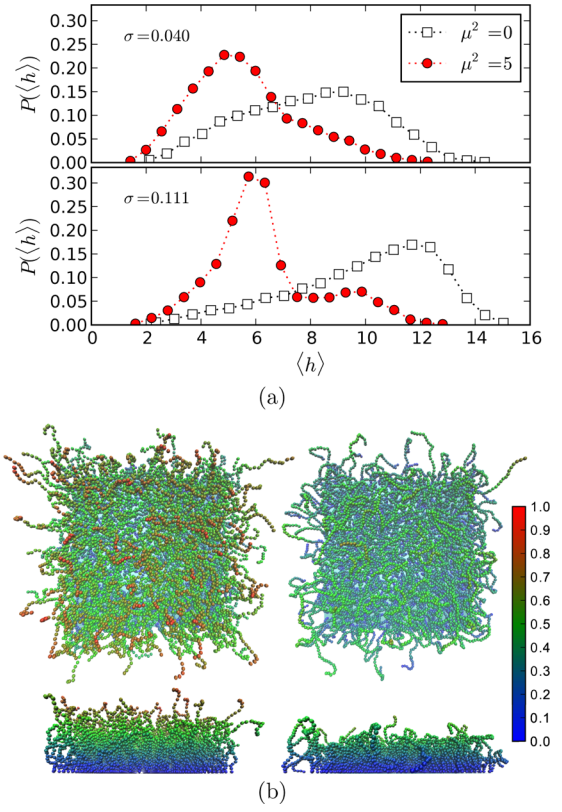

Figure 4. (a) Comparison of the probability distributions of the mean height of chains with length N = 30 obtained for magnetic and nonmagnetic brushes with two selected grafting densities. (b) Top and side views of typical nonmagnetic (left) and magnetic (right) brushes. The color scale indicates the z coordinate of the center of every individual bead, relative to the characteristic contour length of the chains, $(N-1)d$. These examples correspond to the parameters N = 30, σ = 0.111, μ^2 = 0 and 5.

obtained for brushes of chains with length N = 30 and two selected grafting densities. As it is expected, the magnetic brushes show a clear shift of the curves toward lower heights when compared to the corresponding magnetic case. The latter shows a single maximum whose position tends to shift toward higher values as the grafting density grows, and consequently, the steric repulsion forces the chains to adopt more vertically extended conformations. More interestingly, for high values of the grafting density, the dipolar brush develops a second maximum in its distribution of mean heights. This second maximum is located at higher values and its origin is the enhanced crowding of the region near the grafting surface: since the dipolar brush is more compact in such lower regions,

DOI: 10.1021/acs.macromol.5b01086
Macromolecules 2015, 48, 7658−7669

it more easily reaches a saturation value in its local bead density. As the grafting density grows, more free ends of the chains are expelled from the lower crowded region and forced to dangle above it. Finally, the difference in heights between magnetic and nonmagnetic brushes can be better visualized in Figure 4b, where two examples of typical brush configurations are depicted with a height color scale.

Response to an External Magnetic Field. In order to check if the density profile can be effectively manipulated with an external magnetic field, we performed an additional set of simulations in which fields with different strengths were applied perpendicular to the grafting surface, $\vec{H} = H\hat{k}$. In this way, we expect that, once the interaction of the dipoles with the field becomes strong enough to overcome the thermal fluctuations and the magnetic dipole−dipole interaction between the beads, the chains will experience a vertical extension in order to maximize their alignment with the direction of the field. As a result, the thickness of the brush will steadily increase with the field strength, up to the point where the end-to-end distance approaches the chain contour length. An example of such an evolution of the density profile is provided in Figure 5a. The zero-field density profile, with its characteristic −1.3-power tail, evolves into a basically rectangular distribution with growing field. Initially, this evolution is rather slow due to the dominance of dipolar bead−bead interactions and the internal structure of the brush (which, for zero field, will be explained in detail in the next Section). As the field-dipole coupling becomes stronger, the internal structure of the brush simplifies drastically, as the chains tend to straighten and coalign with the external field, avoiding any entanglements. The alignment of the bead dipoles leads to the change of the average brush magnetization, $\langle M \rangle$. This parameter is defined as the total magnetic moment of the system projected on the direction of the external field:

$$\langle M \rangle = \langle \sum_{i=0}^{N_T} \vec{\mu}_i \cdot \hat{k} \rangle \tag{10}$$

where N_T is the total number of beads in the system, and $\vec{\mu}_i \cdot \hat{k}$ denotes the z coordinate of the magnetic moment of bead i. The averaging is performed over all sampled configurations. Note that in these simulations the dipole moments of the grafted beads are always pointing perpendicular to the grafting surface (i.e., parallel to the field). This means that the zero-field magnetization of the brush cannot be strictly zero. In the following, we subtract the zero-field magnetization from the total, $\langle M^* \rangle = \langle M \rangle_H - \langle M \rangle_{H=0}$. In Figure 5b, we present the change of this parameter with growing field. As it can be observed, the magnetization of the brush grows and approaches a plateau, corresponding to the value of the saturation magnetization. For an individual chain, one can predict the equilibrium magnetization using the model proposed by Mendelev and Ivanov for self-assembled, not cross-linked chains of magnetic particles.[57] The result is shown in the same figure with a solid line. The agreement between the simulation data and the analytical approach is rather good, even though the latter is a very rough description of the magnetization of a magnetic filament due to its disregard of the cross-links. Even more surprising is that the analytical model, in which the interparticle correlations are underestimated, predicts higher values of the magnetization for small values of H. In a previous work,[33] we showed that the initial susceptibility of a magnetic filament is enhanced by the presence of the permanent bonds. In the brush, however, this effect seems to be suppressed. It can be explained looking at the first moment of the density profiles, also plotted in Figure 5b. As one can see, the qualitative change of the average brush height and the brush magnetization with growing field is basically the same. On the one hand, the observed height-magnetization coupling can be attributed to a strong correlation between the direction of the dipole and the orientation of the chain backbone. On the other hand, the fact that the average chain height is changing at a slower rate than the magnetization at low field strength indicates the presence of a complex internal structure of the brush caused most probably by the interchain interactions. The upper boundary of the field range, for which the complex internal structure of the brush turns out to be important and makes the chain straightening difficult, can be localized by looking at the point where the analytical curve and the simulation data cross. After this point, the simulated magnetization becomes higher than the analytical prediction. This crossover takes place due to the reduction of the interchain interaction caused by the straightening of the chains.

Finally, it is worth mentioning that the system studied here has a stronger response not only with respect to polyelectrolyte brushes with extended electric dipoles, as discussed above, but also in comparison to former systems that have magnetic colloids embedded within the polymer brush structure.

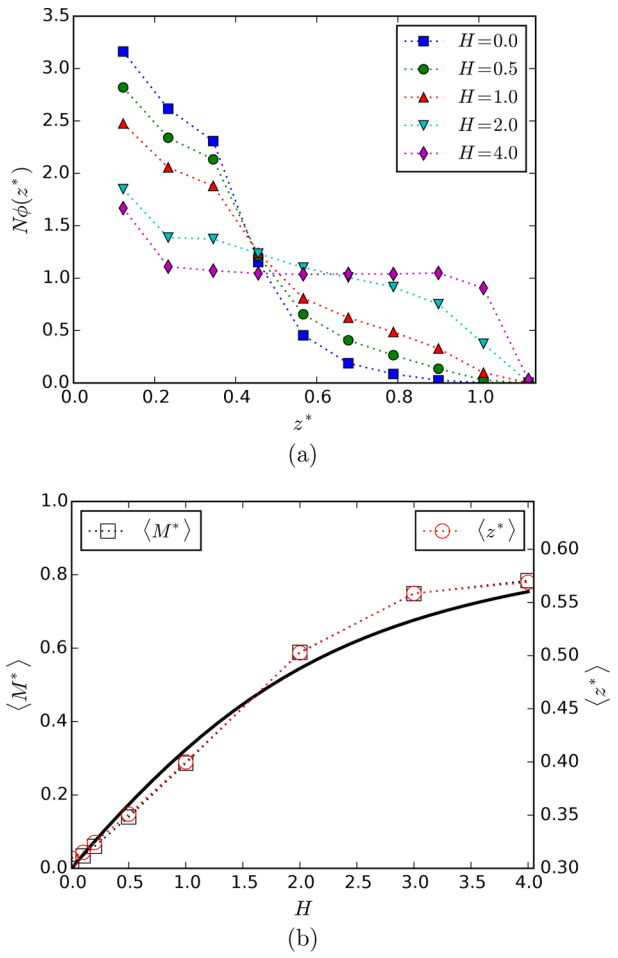

Figure 5. (a) Density profiles for different values of an applied external dimensionless magnetic field, H. (b) Reduced magnetization, $\langle M^* \rangle$ (simulations with circles and theoretical model with a solid line), and the first moment of the simulated density profile, $\langle z^* \rangle$ (squares), as a function of H. Both plots are for $N = 10$, $\sigma = 0.111$, $\mu^2 = 5$.

DOI: 10.1021/acs.macromol.5b01086
Macromolecules 2015, 48, 7658−7669

For instance, in the experimental study of Choi and coworkers[19] or the computational one of Ye et al.,[20] the maximum extension of the brush thickness under an applied external magnetic field did not exceed 30%. In our case, according to the values of $\langle z^* \rangle$ shown in Figure 5b, the thickness of a magnetic filament brush is expected to change by almost a factor of 2. These differences in the change of the thickness are mainly a consequence of the higher compactness of the magnetic filament brush under weak and zero field conditions.

With this discussion we have proven that, in order to fully understand the behavior of the filament brush magnetic response and its enhanced structural change, it is essential to look at the free field case, where the interparticle correlations are not affected by the presence of an external force. In order to unveil this point, we need to analyze other observables with a higher structural resolution. This analysis is performed in the next sections.

PROPERTIES ON THE PARTICLE SCALE

Here, we scrutinize the zero-field structure of the brush on the level of chain beads. In this way, we are able to analyze local fluctuations and pinpoint the part of the pure dipolar interaction in the A-type Stockmayer brush microstructure, avoiding the inherent contribution from charges present in the aforementioned model of polyelectrolyte brushes.[35] In simulations, chains can stretch and shrink somewhat, due to the presence of springs and soft core interactions between neighbors (see, eqs 2−4). Apart from these permanent links, particles from both the same chain and from neighboring chains can come in close contact forming clusters. Our analysis is based on the characterization of such clusters by means of an approach based on graph theory.

Connectivity Network Analysis. First, we introduce the parameters we chose for the characterization of the brush microstructure. Let us look individually at beads forming the chains in the brush. These beads unavoidably interact with each other via both dipolar and steric interactions, independently from being or not permanently bonded. The interplay of these interactions and thermal fluctuations leads to a complex equilibrium self-assembly of the beads within the brush. In order to classify these structures formed by individual beads, we introduce a criteria of two beads forming a cluster: two beads are connected if, and only if, the distance between them is smaller than a certain r_c. Here, we set r_c to be the maximum length among all permanent bonds observed in the simulation measurements for a given brush. In this way, all permanently bonded particles are considered connected, but additional connections may also form in each configuration. In order to reduce the computational load of the calculations, and taking into account that here we are only interested in a qualitative comparison between the magnetic and the nonmagnetic cases; in this and the next sections, we do not consider the lateral periodic boundaries when computing the distances between beads belonging to different chains. However, checks shown that the periodicity of the system equally affects magnetic and nonmagnetic brushes and does not qualitatively influence the results provided below.

In order to classify the connections between different beads and to create its convenient graphical representation, we employ a standard algorithm from the graph theory[58] to build a so-called adjacency matrix, $\mathbf{A} = \{a_{i,j}\}$. This matrix has a dimension $N_T \times N_T$. The elements of $\mathbf{A}$ are $a_{i,j} = 1$ if beads i and j are connected, and $a_{i,j} = 0$ otherwise. On the basis of such a matrix, one can build a graph of the connected beads, in which all beads form a set of vertices and their connections serve as edges. Two examples are visualized in Figure 6. Upper images show the graph representation of randomly chosen configurations from the simulation data of the brush with $\sigma = 0.04$, $N = 15$. One can see that the amount of clusters different from isolated chains (the number shown in the corner) is much higher if no magnetic interaction is present (right, framed with gray). To show the topology of the brush in real space, in the lower row we provide the snapshots corresponding to the visualized adjacency matrices. All clusters that have connectivity $N - 1$ (isolated chains) are semitransparent, whereas every other cluster is colored differently. Figure 6 shows how the presence of noncentral interaction, which favors head-to-tail or antiparallel orientation of dipoles (left, framed with red), reduces the probability of the formation of bulky interlaced clusters with multiple branching points. For the magnetic brush, one can see the presence of a ring-like structure, as well as longer linear clusters. The only way to form an extended linear aggregate is when the chain folds and attaches its free end to the grafted bead of a neighboring chain. This type of fold can explain the higher density of the magnetic brush near the grafting surface that was evidenced by the profiles $\phi(z)$ in the previous section. Since the choice of the configuration was essentially random, it is more reliable to analyze some thermodynamically averaged characteristics. To do so, we chose the observables presented in Figure 7. The first quantity is the number of edges in the graph (ones in the adjacency matrix) averaged over all sampled configurations. The edges are drawn with solid black lines. To confirm that the dipolar interaction inhibits the formation of bulky clusters with multiple junctions, we study the average degree δ of the vertices, i.e., the average number of edges connected per vertex (see arrows in Figure 7). Besides this, in

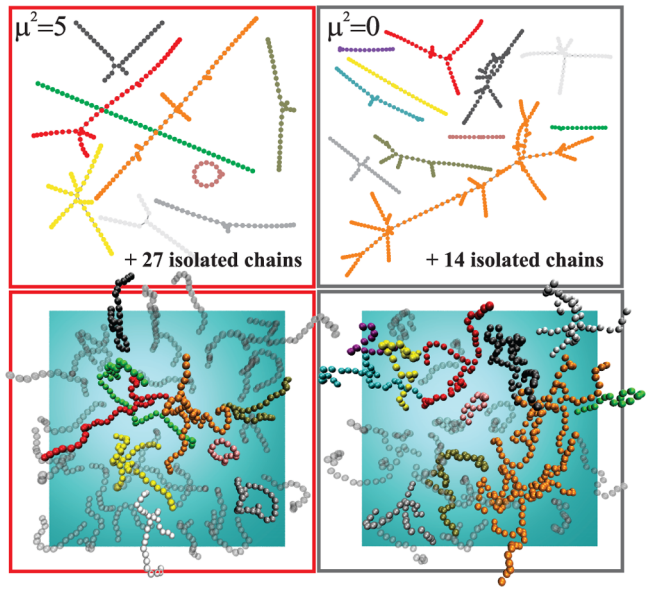

Figure 6. Graphical representation of adjacency matrices (upper row) and corresponding simulation snapshots (lower row). On the left, we visualize the configuration of a magnetic filament brush with $N = 15$ and $\sigma = 0.04$; on the right, the configuration for a nonmagnetic brush with the same chain length and grafting density is presented. Isolated chains are not shown explicitly in the graphical representation: their numbers are provided in the corners. In order to underline the difference in the cluster topology, we present each cluster with a different color. In the snapshots, all isolated chains are semitransparent.

DOI: 10.1021/acs.macromol.5b01086
Macromolecules 2015, 48, 7658−7669

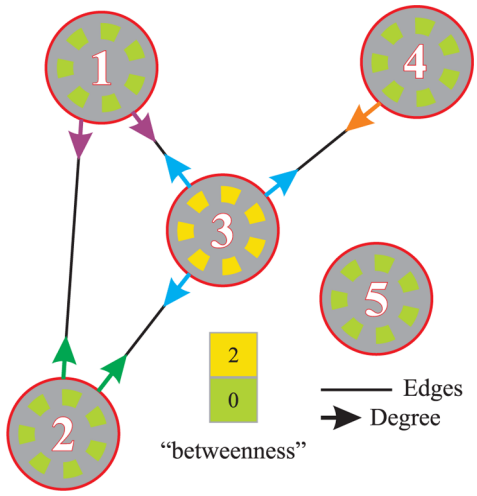

Figure 7. Sketch of a connectivity graph. Numbered circles represent the vertices, black lines the edges. The degree of each vertex corresponds to the number of outcoming colored arrows. The color of the dashed circles within the vertices indicates its betweenness.

order to estimate the importance of a certain vertex in the network of connections, we perform the analysis of the so-called centrality. In particular, we use betweenness,[59−61] which is a standard tool used to characterize nodes in graph theory. In order to describe this parameter, let us first introduce the concept of path. If V is the set of vertices, and u and w are two randomly chosen members of this set, then the edges you need to walk from u to w form a path. There might be many ways to walk from u to w, thus, for any two vertices there exists a set of paths. The shortest path is the one containing the minimal amount of edges. Using this formalism, the betweenness of a vertex v which belongs to the set of vertices V of the clustered brush, can be computed as the ratio:

$$C_B(v) = \sum_{u,w \in V} \frac{p^s_{uw}(v)}{p^s_{uw}} \tag{11}$$

where p^s_{uw} is the total number of shortest paths between vertices u and w, and $p^s_{uw}(v)$ is the number of those paths that pass through v. The betweenness is shown in Figure 7 with dashed circles, whose color corresponds to the value indicated in the legend. In that example, the shortest path between 1 and 4, as well as the one between 2 and 4, goes through 3. All other vertices are either directly connected or totally disconnected, as is the case of v = 5, so their betweenness is zero.

Brush Microstructure. We begin our analysis of the brush structure at the bead scale by addressing the changes in the vertices degree, δ. For the initial configuration (a brush with straight vertical chains of length N), the distribution of the degrees is evident: all free ends (whose number is N_T/N) have δ = 1; all grafted ends also have δ = 1; the remaining beads (in the amount N_T $(1 - 2/N)$) have δ = 2. In a thermodynamically equilibrated brush, the chain beads can have a higher degree, depending on how many added nearest neighbors they have as a consequence of thermal fluctuations or magnetic dipole−dipole interparticle interactions. The histograms of δ for the initial brush configurations and for thermodynamically equilibrated brushes obtained for selected values of N, σ, and for both μ^2 = 0 and 5, are presented in Figure 8. It can be easily seen that the width of the histograms is broader for nonmagnetic brushes (front) with respect to that of the magnetic filament brush (middle). In general, the degree of vertices is growing with increasing grafting density for both brushes as a consequence of the increasing combinatoric probability for two particles to form a connection (additional edge). However, looking at these histograms, one can say that the assumption for dipolar forces to work against the formation of bulky clusters and multiple junctions (first noticed in Figure 6) becomes more grounded. In order to elucidate the nature of the redistribution of degrees, we analyze the behavior of the free and the grafted ends of the filaments. The results are summarized in Table 2. It becomes evident that the presence of the magnetic dipole−dipole interaction significantly strengthens the role of both free and grafted ends in the cluster formation. For a grafted end to take part in the cluster, it is essential that a neighboring chain

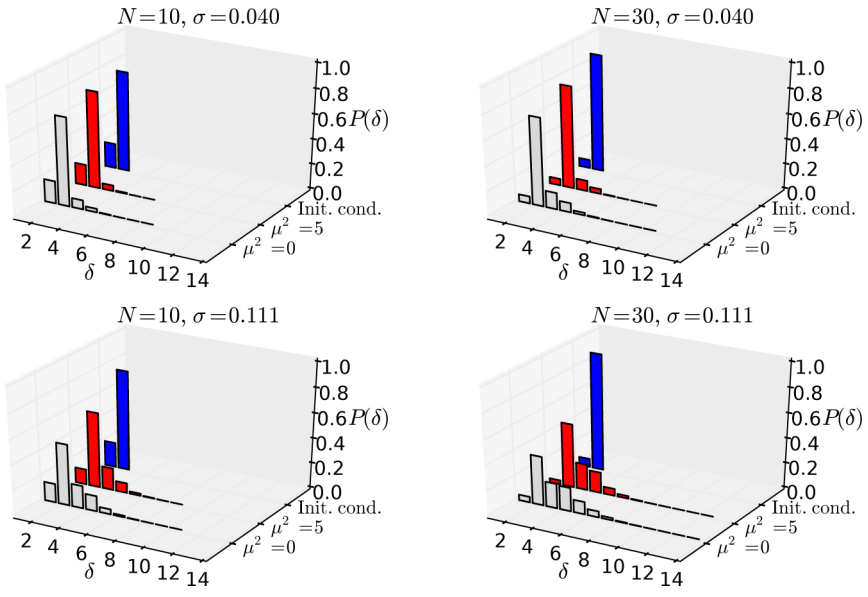

Figure 8. Histograms of the vertices degree corresponding to two selected chain lengths and grafting densities. Histograms in the back correspond to the initial, out of equilibrium configurations; the ones in the middle, to the magnetic brush; in the front, we show the histograms for the nonmagnetic brush.

DOI: 10.1021/acs.macromol.5b01086
Macromolecules 2015, 48, 7658−7669

Table 2. Characteristic Degrees of Free and Grafted Ends[a]

N	σ	μ^2	free ends, δ	grafted ends, δ
10	0.040	0	1.22	1.05
10	0.040	5	1.25	1.12
10	0.111	0	1.69	1.16
10	0.111	5	1.83	1.39
30	0.040	0	1.40	1.07
30	0.040	5	1.42	1.15
30	0.111	0	2.09	1.25
30	0.111	5	2.11	1.59

[a]Relative error intervals do not exceed 5%.

bends and attaches either its free end or any other bead to it. Alternatively, the chain, whose grafted end has $\delta > 1$, bends by itself to connect one of the beads to the grafted one (examples can be found in Figure 6). In both cases, these two configurations effectively increase the density of beads near the grafting surface and decrease the average height of a brush made of magnetic filaments.

In order to estimate the total number of newly formed connections within the brushes, we plot in Figure 9 the average

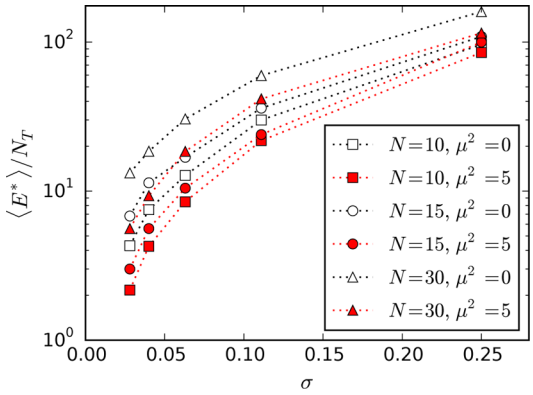

Figure 9. Average number of newly formed edges as a function of σ. Red filled symbols correspond to magnetic filament brushes, open symbols to nonmagnetic ones. The last two points for $N = 30$ are extrapolated. We use a log scale for the ordinate axis.

number of non permanent edges in the adjacency matrix, $\langle E^* \rangle$, normalized by the total number of particles, N_T, as a function of grafting density for various chain lengths. Note that we obtain $\langle E^* \rangle$ by subtracting permanent bonds from the total amount of edges and focus on the temporary connections only. It is of course expected that, for both magnetic and nonmagnetic brushes, the amount of edges grows rapidly with the grafting density. However, the total amount of edges formed in a nonmagnetic brush is higher than the one in a brush made of magnetic filaments. This can be explained by the selectivity of the connections in the magnetic case: there is only a limited volume of space around each bead to where a second one could be attracted (and a part of this volume is already occupied by the permanent neighbors). The attempt of establishing a new connection from outside of such favorable regions results in a strong dipolar repulsion between the beads. In such a way, magnetic forces prevent the formation of random connections and stimulate the formation of energetically advantageous ones, whose amount is relatively low.

In order to understand how this anisotropy of the magnetic dipolar interaction influences the overall connectivity of the networks and clusters, as the final step, we study the centrality of the connections. In Figure 10, we present two different types of plots in four panels. In the upper panels the results for $N = 10$ are presented, whereas lower panels correspond to $N = 30$. The left side corresponds to $\sigma = 0.04$, the right one is for $\sigma = 0.111$. First, we focus on the lower part of each panel, where one can see the plots of the average betweenness for each particle in the system (the bead indices can be seen along the horizontal axes). In these plots, gray lines describe the nonmagnetic brush, whereas the red lines characterize the brush made of magnetic filaments. The overall parabolic profiles of the curves come as a consequence of the brush' finite size. In addition, one can clearly see two types of periodicity in these graphs. In order to understand these periodicities, one needs to know the way the indices are assigned to the particles. For example, in case of $\sigma = 0.04$ and $N = 10$, the particle with zeroth index is the free end of the first chain; the particle with index 9 is the grafted bead of the first chain. To determine the position of a particle with index p, one needs to calculate first $[p/N] + 1$ (with $[\cdot]$ denoting the integer part), this defines the number of the chain to which the particle belongs; next, the $\mathrm{res}(p/N) + 1$ (with $\mathrm{res}(\cdot)$ denoting the residue of the division) will provide the position within the chain from the free end. According to this assignment, the shorter period in the curves corresponds to the distribution of C_B along individual permanent chains (grafted and free ends tend to have a lower value than the middle parts). The larger period is another manifestation of the system finite size: it reflects the distance to the edges of the simulation box of the grafting positions of the permanent chain to which the given bead belongs. For short chains and low grafting densities, the overall entanglement of the brush is very low, that is why the value of betweenness is weakly dependent on the grafting position of the corresponding permanent chain. The different periods become more evident as the structure becomes more entangled. More importantly, the plots of the average betweenness of each particle show that beads in magnetic filament brushes have higher betweenness (notice the dominance of gray lines at low values). In order to understand where this difference stems from, one needs to look at the upper plots. Here, we present the average distribution of betweenness along positions in the chains. Chain particles are drawn explicitly along the vertical axes, with the grafted bead in the bottom and the free end on the top. In this way, the horizontal axis indicates the value of betweenness (growing to the right for the magnetic brush and to the left for the nonmagnetic one). Color gradients are used to represent the number of particles with the given value of C_B at the corresponding position along the chain. The lighter is the color, the less beads had the respective betweenness. In the initial configuration, when all chains are straight pointing perpendicular to the grafting surface, the betweenness of each chain bead at the position k can be calculated as

$$C_B^{sc}(k) = -k^2 + (N+1)k - N \tag{12}$$

where $k = 1, \ldots, N$ and N is the number of particles in the permanent chain. Expression 12 is obtained by simple combinatoric considerations: for a given bead k in an isolated chain of length N, one can find other $k - 1$ beads in one of the directions along the chain; from each of those latter beads, there is a path that passes through k to the $N - k$ beads that are in the opposite direction. The expression in eq 12 reflects the symmetry of the chain with respect to its central bead and its graphical representation is shown as solid lines in the upper left plot of Figure 10. For the other three cases (higher N and σ) the results of the eq 12 for the initial configurations would not be

DOI: 10.1021/acs.macromol.5b01086
Macromolecules 2015, 48, 7658−7669

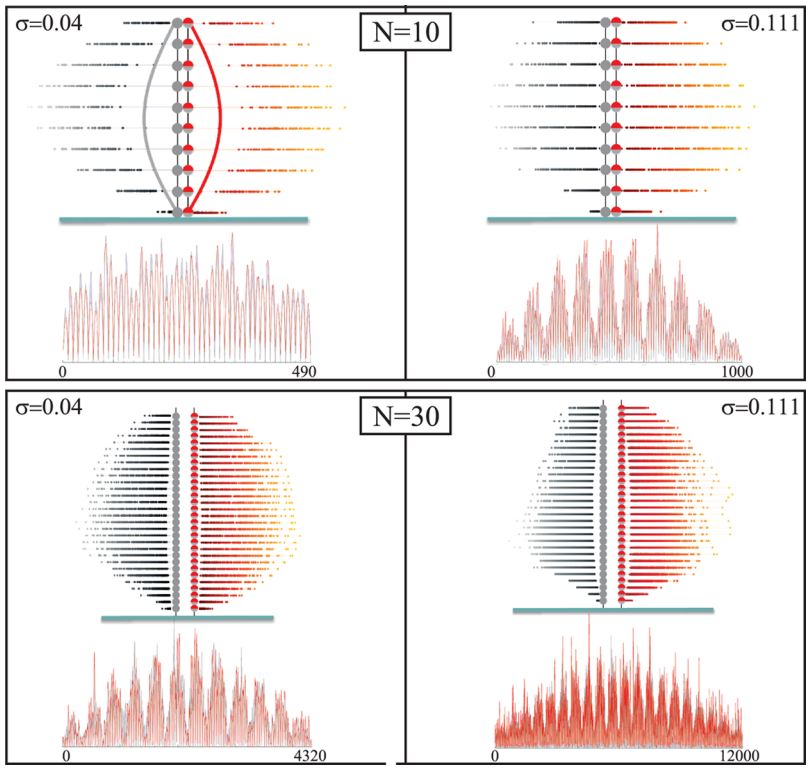

Figure 10. Betweenness. Upper panels are for $N = 10$; lower panels are for $N = 30$. Left panels are obtained for $\sigma = 0.04$; right ones for $\sigma = 0.111$. In the lower parts of each panel, the betweenness (averaged over all sampled configurations) is plotted for each particle in the brush (gray lines for a nonmagnetic system, red lines for a brush made of magnetic filaments). The numbers along the horizontal axes are the beads indices. In the upper parts of the panels, we plot the distributions of betweenness depending on the position of the bead within the permanent chain, which is sketched along the vertical axes of the plots (magnetic on the right, gray/red; nonmagnetic on the left, gray). Horizontal rectangles at the bottom of the chains represent the grafting surface. The parabolas in the upper left panel ($N = 10$ and $\sigma = 0.04$) characterize the betweenness for the initial configuration with straight chains; corresponding parabolas for the other parameters cannot be seen in the provided scale.

distinguishable from zero in the scales used in the plots. The betweenness for particles in the equilibrated brush is always higher than the one of the initial configuration due to the growing amount of nonpermanent connections. A more interesting observation is that the betweenness of the grafted ends is significantly higher in the magnetic filament brush than in the nonmagnetic one. For the latter, the grafted beads rarely end up being between any others. This behavior qualitatively does not change with growing grafting densities and chain lengths. Therefore, the fact that one sees gray lines close to the horizontal axes in the plots of the average betweenness for each particle (lower plots) is explained by the lower connectivity of the grafted ends in the nonmagnetic case. Finally, the distributions of betweenness along the chains also evidence that, in general, $C_B(k)$ is higher in the magnetic filament brush and has a less pronounced maximum when approaching the middle of the chain. These results confirm the assumption of the strong directional clustering in magnetic filament brushes.

The fact that the grafted and the free ends actively participate in the bead self-assembly within the magnetic filament brush not only explains the reason for it to be more compact but also why a weak external magnetic field cannot yield high magnetization. For a brush to reach the saturation magnetization, it is essential that all chains become almost straight. Therefore, the field should be high enough to prevent the strong bending of the filaments produced by the dipolar entanglements, in which the free and grafted ends take an important role.

CONCLUSION

In this manuscript, we presented the results of a combined theoretical−computational study of magnetic supramolecular filament brushes. The interest of this system lies in the possibility to control the structural behavior of the brush with an external magnetic field of a moderate strength. This perspective opens up a broad range of new applications in different fields, such as chromatography and microfluidics. The first step on this way was to understand the fundamental difference brought by the magnetic interactions and the structure of head-to-tail cross-linked dipoles that form the filaments to a polymer brush-like system. In order to do this, we compare by means of Langevin dynamics simulations the behavior of magnetic filament brushes to that of nonmagnetic neutral brushes, polyelectrolyte brushes with extended electric dipoles and polyelectrolyte brushes with embedded magnetic colloids. It is worth mentioning that the differences brought by the magnetic interactions become evident already at the filament scale: in contrast to a nonmagnetic filament brush or to the one made out of polyelectrolyte chains, both with parabolic density distributions, the magnetic brush with the same grafting density is denser close to the substrate but it has a clear −1.3-power tail at farther distances. This results in bimodal height distributions for dense magnetic brushes, whereas regular brushes exhibit unimodal profiles. This difference is more pronounced as the length of the chains that form the brush increases. This is not true for a polyelectrolyte brush with extended dipoles, for which the role of the dipolar interactions gets screened with

DOI: 10.1021/acs.macromol.5b01086
Macromolecules 2015, 48, 7658−7669

increasing grafting density. It turned out that the zero-field internal structure of a magnetic filament brush has a crucial influence on the magnetic response of these systems. If a weak external magnetic field is applied, the magnetic response of the filament brush is partially hindered by the interchain interactions within the compact region near the grafting substrate. However, if the field is strong enough to compete with the interparticle magnetic dipole−dipole interaction and thermal fluctuations, then the total magnetization fast reaches a value close to its saturation due to an almost complete straightening of the chains. The latter results in a pronounced change of the density profiles.

In order to elucidate both the reasons for the magnetization hindrance under low fields and the different behavior of the magnetic and nonmagnetic brushes at the scale of individual chain beads, we employed graph theory. We performed a cluster analysis by introducing the concept of connected beads, according to a simple distance criterium. On the basis of this approach, the brush was presented as a graph, in which the number of edges (connections), the degree of vertices and the peculiarities of the connectivity were carefully analyzed for various grafting densities and chain lengths in both magnetic and nonmagnetic cases. We found that magnetic interactions act against random density fluctuations, and on average the number of connections in the magnetic brush is lower than in a nonmagnetic one, albeit both grow with the grafting density. The dominant connective unit in the dipolar brush, except for the highest grafting density, is a bead with only two neighbors. It was found that free ends in a dipolar brush also tend to have a second neighbor. To allow this, a chain has to bend, frequently to connect to the grafted bead of a neighboring chain. This is also confirmed by centrality analysis: free ends in a dipolar brush have a higher degree of betweenness than in the case of a nondipolar brush. For the latter, the distribution of degrees is shifted toward higher values, and the probability for a bead to have more than two neighbors simply grows with increasing grafting density. At the same time, the betweenness for free ends of nondipolar brush is rather low due to the absence of any directional interaction.

Note that the long-range nature of magnetic dipole−dipole interaction results in a qualitative change in the behavior of a brush, which cannot be obtained by introducing a simple angular dependent short-range potential between chain beads. The dipolar forces between beads in one chain effectively lead to local stiffening, but also result in long-range anisotropic interchain interactions. The latter plays a crucial part in the brush microstructure. Neither the same kind of behavior can be achieved by using extended electric dipoles, as this will lead to the dominance of central Coulomb interaction at short distances on growing grafting density. Besides that, the magnetic filament brush proposed here shows a much stronger height change under the influence of an applied external magnetic field in comparison to previously studied systems.

In future, we plan to develop a theoretical approach to describe the density profile of a magnetic filament brush. It is also essential to perform a detailed study of the chain parameters, such as dipolar strength and angular bond rigidity, as well as determine the influence of the temperature on the equilibrium structure of the system.

AUTHOR INFORMATION

Corresponding Author

*(P.A.S.) E-mail: pedro.sanchez@univie.ac.at.

Notes

The authors declare no competing financial interest.

ACKNOWLEDGMENTS

This research has been partially supported by the Austrian Research Fund (FWF): START-Projekt Y 627-N27. The authors are grateful to the Ural Federal University stimulating programme. S.S.K, E.S.P., and E.V.N. are supported by RFBR mol-a-ved 15-32-20549. The work of E.V.N. was partially supported by the President of RF, Grant NO MK-5216.2015.2. S.S.K. is supported by the Ministry of Education and Science of the Russian Federation (Contract 02.A03.21.000, Project 3.12.2014/K) and EU-Project 642774 ETN-Colldense. P.A.S. acknowledges financial support from the Universitat de les Illes Balears within its Programa de foment de la recerca. T.S. and J.J.C. were supported by the project FIS2012-30634 (funded by the Spanish Mineco). J.J.C. and T.S. also acknowledge funding from a grant awarded by the Conselleria d'Educació, Cultura i Universitats del Govern de les Illes Balears and the European Social Fund (ESF). Computer simulations were performed at the Vienna Scientific Cluster (Austrian universities consortium for High Performance Computing) and the Nuredduna high-throughput computing cluster (IFISC, UIB-CSIC). We thank Michaela McCaffrey for aesthetic corrections.

REFERENCES

(1) Milner, S. T. *Science* **1991**, *251*, 905−914.
(2) Halperin, A.; Tirrell, M.; Lodge, T. *Macromolecules: Synthesis, Order and Advanced Properties*; Advances in Polymer Science; Springer: Berlin and Heidelberg, Germany, 1992; Vol. *100/1*, pp 31−71.
(3) Azzaroni, O. *J. Polym. Sci., Part A: Polym. Chem.* **2012**, *50*, 3225−3258.
(4) Napper, D. *J. Colloid Interface Sci.* **1977**, *58*, 390−407.
(5) Balazs, A. C.; Singh, C.; Zhulina, E.; Chern, S.-S.; Lyatskaya, Y.; Pickett, G. *Prog. Surf. Sci.* **1997**, *55*, 181−269.
(6) Szleifer, I. *Curr. Opin. Solid State Mater. Sci.* **1997**, *2*, 337−344.
(7) Senaratne, W.; Andruzzi, L.; Ober, C. K. *Biomacromolecules* **2005**, *6*, 2427−2448.
(8) Lin, Y.-H.; Teng, J.; Zubarev, E. R.; Shulha, H.; Tsukruk, V. V. *Nano Lett.* **2005**, *5*, 491−495.
(9) Usov, D.; Gruzdev, V.; Nitschke, M.; Stamm, M.; Hoy, O.; Luzinov, I.; Tokarev, I.; Minko, S. *Macromolecules* **2007**, *40*, 8774−8783.
(10) Takei, Y. G.; Aoki, T.; Sanui, K.; Ogata, N.; Sakurai, Y.; Okano, T. *Macromolecules* **1994**, *27*, 6163−6166.
(11) Merlitz, H.; He, G.-L.; Wu, C.-X.; Sommer, J.-U. *Phys. Rev. Lett.* **2009**, *102*, 115702.
(12) Bünsow, J.; Kelby, T. S.; Huck, W. T. S. *Acc. Chem. Res.* **2010**, *43*, 466−474.
(13) Ouyang, H.; Xia, Z.; Zhe, J. *Nanotechnology* **2009**, *20*, 195703.
(14) Weir, M. P.; Heriot, S. Y.; Martin, S. J.; Parnell, A. J.; Holt, S. A.; Webster, J. R. P.; Jones, R. A. L. *Langmuir* **2011**, *27*, 11000−11007.
(15) Ho, Y.-F.; Shendruk, T. N.; Slater, G. W.; Hsiao, P.-Y. *Langmuir* **2013**, *29*, 2359−2370.
(16) Tong, C. *Langmuir* **2014**, *30*, 15301−15308.
(17) Kamachi, M. *J. Macromol. Sci., Polym. Rev.* **2002**, *C42*, 541−561.
(18) Blundell, S. J.; Pratt, F. L. *J. Phys.: Condens. Matter* **2004**, *16*, R771−R828.
(19) Choi, W. S.; Koo, H. Y.; Kim, J. Y.; Huck, W. T. S. *Adv. Mater.* **2008**, *20*, 4504−4508.
(20) Ye, Y.; Pan, Z.; Zhang, L.; He, L.; Xia, A.; Liang, H. *J. Polym. Sci., Part B: Polym. Phys.* **2010**, *48*, 1873−1881.
(21) Dreyfus, R.; Baudry, J.; Roper, M. L.; Fermigier, M.; Stone, H. A.; Bibette, J. *Nature* **2005**, *437*, 862−865.
(22) Benkoski, J. J.; Bowles, S. E.; Jones, R. L.; Douglas, J. F.; Pyun, J.; Karim, A. *J. Polym. Sci., Part B: Polym. Phys.* **2008**, *46*, 2267−2277.
(23) Ērglis, K.; Zhulenkovs, D.; Sharipo, A.; Cēbers, A. *J. Phys.: Condens. Matter* **2008**, *20*, 204107.
(24) Zhou, Z.; Liu, G.; Han, D. *ACS Nano* **2009**, *3*, 165−172.

DOI: 10.1021/acs.macromol.5b01086
Macromolecules 2015, 48, 7658−7669

(25) Byrom, J.; Han, P.; Savory, M.; Biswal, S. L. *Langmuir* **2014**, *30*, 9045−9052.
(26) Singh, H.; Laibinis, P. E.; Hatton, T. A. *Nano Lett.* **2005**, *5*, 2149−2154.
(27) Cēbers, A. *Curr. Opin. Colloid Interface Sci.* **2005**, *10*, 167−175.
(28) Belovs, M.; Cēbers, A. *Phys. Rev. E* **2009**, *79*, 051503.
(29) Fahrni, F.; Prins, M. W. J.; van IJzendoorn, L. J. *Lab Chip* **2009**, *9*, 3413−3421.
(30) Babataheri, A.; Roper, M.; Fermigier, M.; du Roure, O. D. *J. Fluid Mech.* **2011**, *678*, 5−13.
(31) Javaitis, I.; Zilgalve, V. *Adv. Mater. Res.* **2011**, *222*, 221−224.
(32) Cerdà, J. J.; Sánchez, P. A.; Sintes, T.; Holm, C. *Soft Matter* **2013**, *9*, 7185−7195.
(33) Sánchez, P. A.; Cerdà, J. J.; Sintes, T.; Ivanov, A. O.; Kantorovich, S. S. *Soft Matter* **2015**, *11*, 2963−2972.
(34) Srivastava, S.; Nykypanchuk, D.; Fukuto, M.; Halverson, J. D.; Tkachenko, A. V.; Yager, K. G.; Gang, O. *J. Am. Chem. Soc.* **2014**, *136*, 8323−8332.
(35) Kaznessis, Y. N.; Hill, D. A.; Maginn, E. J. *Macromolecules* **1998**, *31*, 3116−3129.
(36) Weeks, J. D.; Chandler, D.; Andersen, H. C. *J. Chem. Phys.* **1971**, *54*, 5237−5247.
(37) Murat, M.; Grest, G. S. *Macromolecules* **1989**, *22*, 4054−4059.
(38) Gauger, E.; Stark, H. *Phys. Rev. E* **2006**, *74*, 021907.
(39) Gauger, E.; Downton, M.; Stark, H. *Eur. Phys. J. E: Soft Matter Biol. Phys.* **2009**, *28*, 231−242.
(40) Abraham, F. F.; Singh, Y. *J. Chem. Phys.* **1977**, *67*, 2384−2385.
(41) Limbach, H. J.; Arnold, A.; Mann, B. A.; Holm, C. *Comput. Phys. Commun.* **2006**, *174*, 704−727.
(42) Arnold, A.; Lenz, O.; Kesselheim, S.; Weeber, R.; Fahrenberger, F.; Roehm, D.; Košovan, P.; Holm, C. In *Meshfree Methods for Partial Differential Equations VI*; Griebel, M., Schweitzer, M. A., Eds.; Lecture Notes in Computational Science and Engineering; Springer: Berlin and Heidelberg, Germany, 2013; Vol. *89*; pp 1−23.
(43) Allen, M. P.; Tildesley, D. J. *Computer Simulation of Liquids*, 1st ed.; Oxford Science Publications Clarendon Press: Oxford, U.K., 1987.
(44) Kubo, R. *Rep. Prog. Phys.* **1966**, *29*, 255.
(45) Cerdà, J. J.; Kantorovich, S.; Holm, C. *J. Phys.: Condens. Matter* **2008**, *20*, 204125.
(46) Kantorovich, S.; Cerdà, J. J.; Holm, C. *Phys. Chem. Chem. Phys.* **2008**, *10*, 1883−1895.
(47) Cerdà, J. J.; Ballenegger, V.; Lenz, O.; Holm, C. *J. Chem. Phys.* **2008**, *129*, 234104.
(48) Bródka, A. *Chem. Phys. Lett.* **2004**, *400*, 62−67.
(49) Rubinstein, M.; Colby, R. H. *Polymer Physics*; Oxford University Press: Oxford, U.K., 2003.
(50) Milner, S. T.; Witten, T. A.; Cates, M. E. *Macromolecules* **1988**, *21*, 2610−2619.
(51) De Gennes, P. G. *Macromolecules* **1981**, *14*, 1637−1644.
(52) Klokkenburg, M.; Vonk, C.; Claesson, E. M.; Meeldijk, J. D.; Erné, B. H.; Philipse, A. P. *J. Am. Chem. Soc.* **2004**, *126*, 16706−16707.
(53) Klokkenburg, M.; Dullens, R. P. A.; Kegel, W. K.; Erné, B. H.; Philipse, A. P. *Phys. Rev. Lett.* **2006**, *96*, 037203.
(54) Sánchez, P. A.; Cerdà, J. J.; Sintes, T.; Holm, C. *J. Chem. Phys.* **2013**, *139*, 044904.
(55) Rovigatti, L.; Kantorovich, S.; Ivanov, A. O.; Tavares, J. M.; Sciortino, F. *J. Chem. Phys.* **2013**, *139*, 134901.
(56) Kantorovich, S.; Ivanov, A. O.; Rovigatti, L.; Tavares, J. M.; Sciortino, F. *Phys. Rev. Lett.* **2013**, *110*, 148306.
(57) Mendelev, V. S.; Ivanov, A. O. *Phys. Rev. E* **2004**, *70*, 051502.
(58) Godsil, C.; Royle, G. *Algebraic Graph Theory*; Graduate Texts in Mathematics; Springer: New York, 2001; Vol. *207*, pp 163−192.
(59) Freeman, L. C. *Sociometry* **1977**, *40*, 35−41.
(60) Newman, M. E. J. *SIAM Rev.* **2003**, *45*, 167−256.
(61) Borgatti, S. P.; Everett, M. G. *Social Networks* **2006**, *28*, 466−484.

DOI: 10.1021/acs.macromol.5b01086
Macromolecules 2015, 48, 7658−7669